Quality-controlled deformation analysis of the 26-m HartRAO radio telescope's main reflector: First results

Theresa PFAFFINGER[*1], **Marco Antonio Ortiz RINCÓN**[1], **Axel NOTHNAGEL**[2], **Philip MEY**[3], **Jonathan QUICK**[3], **Roelf BOTHA**[3], **Pieter STRONKHORST**[3], **Marisa NICKOLA**[3], and **Christoph HOLST**[1]

[1] *Chair of Engineering Geodesy, TUM School of Engineering and Design, Technical University of Munich, Germany, (theresa.pfaffinger, marco.ortiz, christoph.holst)@tum.de*

[2] *Research Area Higher Geodesy, Department of Geodesy and Geoinformation, TU Wien, Austria, axel.nothnagel@tuwien.ac.at*

[3] *National Research Foundation, South African Radio Astronomy Observatory (SARAO) Hartebeesthoek Site, South Africa, (pmey, jquick, rbotha, pstronkhorst, mnickola)@sarao.ac.za*

[*] *corresponding author*

Abstract

Radio telescopes are pivotal in receiving radio frequencies from space. These telescopes, typically featuring parabolic dishes, focus radio waves onto a central receiving point to amplify the incoming signal. The stability of the telescope's main reflector's shape across various orientations is crucial, as deformations can distort the received signal. This study focuses on the 26-meter radio telescope at the Hartebeesthoek Radio Astronomy Observatory (HartRAO) in South Africa. A high-end laser scanner is employed to record the surface of the rotating paraboloid reflector in multiple orientations. The telescope is capable of moving through different declinations and hour angles requiring to measuring 88 different positions of the telescope, to provide a complete picture of the deformations. Fitting models are applied to estimate the shape of the rotating paraboloid from the raw data also considering calibration errors of the laser scanner used. First results for deformation patterns and, therefore, the local deformations of the main reflector are shown.

Keywords: Terrestrial Laser Scanning, Calibration, Misalignments, Systematic Errors, VLBI, Segmentation

1. Motivation

VLBI (very long baseline interferometry) telescopes receive signals from compact extragalactic nuclei such as quasars in the radio frequency domain. By simultaneously observing the same radio source, baselines between the reference points of radio telescopes can be established. This information can then be utilized to monitor plate tectonics and Earth rotation parameters (Nothnagel et al., 1994). In addition to terrestrial investigations, VLBI is also employed to determine the positions and morphology of these natural radio sources. These applications require a level of precision in the millimeter range, which in turn necessitates a corresponding stability of the VLBI telescopes (Holst et al., 2019b).

A prerequisite for optimal signal reception is that the form of the reflectors closely matches the model of a perfect shape, even when aligning with different radio sources. The main reflectors of radio telescopes often have the shape of a paraboloid of revolution. However, external factors such as temperature, wind, and, most notably, the telescope's weight and the resulting gravitational forces influence the shape of the main reflector (Clark and Thomson, 1988; Nothnagel, 2009). Changes in the shape directly relate to signal path variations, which deteriorate VLBI observations in a variety of effects (Holst et al., 2019b). This makes it essential to monitor the deformations of the telescope and the reflectors in particular.

Various approaches have been explored to identify radio telescope deformations, e.g., using terrestrial laser scanners (Holst et al., 2019a), total stations (Sarti et al., 2009) or cameras (Lösler et al., 2019, 2025). E.g., Sarti et al. (2009) used a laser scanner for deformation analysis and made control measurements with a total station that confirmed the results of the laser scanner for VLBI telescopes at Medicina and Noto observatories. Similar approaches using laser scanners have been applied to telescopes in Onsala (Holst et al., 2017) and Effelsberg (Holst and Kuhlmann, 2014), with Holst et al. (2017) also focusing on determining the focal length and local deformations. They place particular emphasis on the misalignments of the laser scanner and investigate different methods to minimize the effects of systematic errors of the laser scanner.

In addition to laser scanning approaches, there are also methods based on camera data. For instance, Lösler et al. (2025) recently conducted a UAV-based photogrammetry study to investigate the radio telescope in Tasmania, Australia. The study analyzed the system's focal length in various positions to evaluate potential deviations and influencing factors.

Similar to the aforementioned radio telescopes, the 26-m telescope at Hartebeesthoek Radio Astronomy Observatory (HartRAO), close to Johannesburg in South Africa, suffers from deformations that need to be quantified. In contrast to the aforementioned radio telescopes, this one has an hour-angle-declination (HA-DEC) mount (Nothnagel, 2009). HA-DEC mounts possess a primary axis which is constructed parallel to the Earth rotation axis. The secondary axis is designed perpendicular to the hour angle axis and always tilts the main reflector in celestial declination. This means that the main reflector encounters gravitational load effects other than those of standard azimuth-elevation-mounts investigated before, e.g., at Medicina, Onsala, or Effelsberg. Consequently, the gravitational load effects are not symmetric for all azimuth angles and do not only depend on elevation angle but vary for all pointing positions in the sky.

With this study, we now want to analyze the deformation behavior of the 26-m HartRAO telescope, again based upon laser scans. Here, as first step of the complete deformation analysis, we focus on the following scientific contributions:

1. developing a measurement concept for deriving the deformation patterns of HA-DEC radio telescopes,
2. developing a workflow for an efficient and automatic preprocessing of the laser scans,
3. presenting first concepts for reducing laser scanner misalignments in the processing steps,
4. discussing preliminary results of deformation patterns and current challenges.

2. Radio telescope, measurement concept and preprocessing

The following section describes first the 26-m HartRAO telescope itself and the measurement concept and shows the preprocessing of the laser scans.

2.1 26-m HartRAO telescope

The 26-m HartRAO telescope in South Africa has the typical design of a Cassegrain telescope, meaning that the main reflector has the shape of a concave paraboloid, which is an important fact for our investigations. The given diameter $D = 25.9\ m$ and the focal ratio $f/D = 0.424$ leads to a nominal focal length of $f = 10.9816\ m$ for the telescope in zenith position (National Research Fundation, 2025). The main reflector consists of 255 individual panels arranged in 7 concentric rings. Figure 1 shows a 3D model of the telescope, including the HA- and DEC-axes and two coordinate systems that will be introduced later.

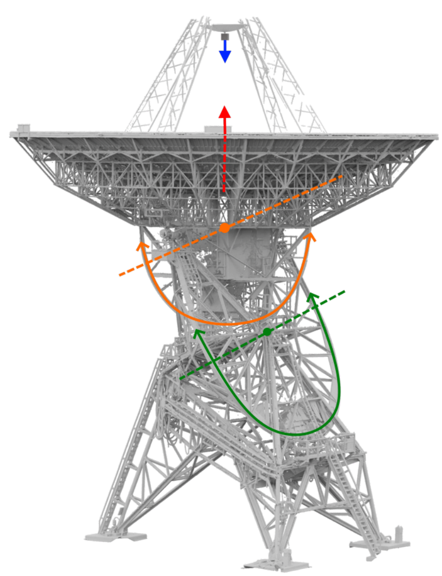

Figure 1. 3D model of the 26-m telescope at the HartRAO site, illustrating the telescope coordinate system's Z-axis (red), the scanner coordinate system's z-axis (blue), the HA-axis in green and DEC-axis in orange.

2.2 Measurement concept

The measurement concept should fulfill some requirements that are necessary for the following processing steps. As the HA-DEC mount should be investigated, it is important that a combination of various positions of the telescope is captured for the analysis. Another prerequisite is that the scanner should scan the main reflector without large occlusions and it should hang always upside-down. The scans should be recorded in a way that the misalignments of the laser scanner can be modeled and minimized in further steps. To fulfill these requirements, the measurement concept is designed as follows.

Laser scanner mounting

To ensure that the whole main reflector can be scanned at each position, a special hinge system is designed, where the scanner is mounted upside down beneath the sub-reflector. This system incorporates a movable two-axis gimbal mechanism, allowing the scanner to remain oriented horizontally toward the nadir in any telescope position due to its weight, shown in Figure 1 and Figure 2.

To ensure stability during scanning, the system has a mechanical brake that restricts the gimbal's movement and locks it when the telescope is in the correct position when activated, preventing unintended motion during the scanning process. The position of the scanner and the hinge system ensures that the whole main reflector is captured in each position except shadows of the quadruped legs and the central cone construction in which various feed horns are mounted (Figure 4 bottom).

Laser scanner misalignments

To model the misalignments of the laser scanner and to minimize the resulting systematic errors in the scans, the scans are taken as two-face scans. Therefore, each position is scanned in two cycles. In cycle 1, the scanner captures data over a horizontal angle range of 0° to 180°, while the vertical angle range is fully covered from 0° to 360°. Cycle 2 repeats the horizontal angle range from 180° to 360°.

As a result, two complementary scans are produced, capturing the entire surface of the telescope's main reflector, except of the obstructed areas. The point clouds that consist of m points, with each point indexed by $j = 1, \ldots, m$, are provided in polar coordinates $[r, \varphi, \theta]$ (range, horizontal angle, vertical angle) with associated intensity values I:

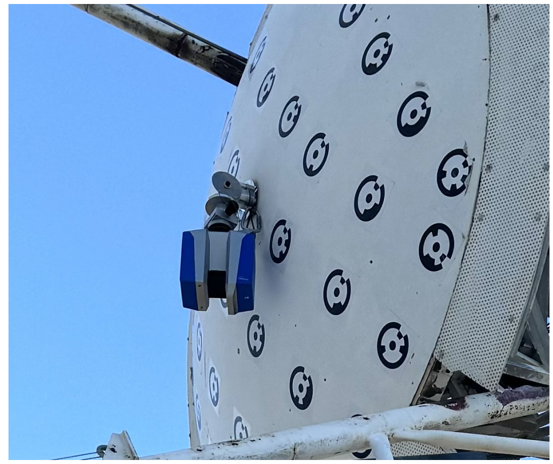

Figure 2. Scanner installation at the sub-reflector with nadir view in the scanner mounting position (HA: −89°, DEC: −1.5°)

$$P_j = \left\{ \mathrm{r}_j, \varphi_j, \theta_j, \mathrm{I}_j \right\}. \quad (1)$$

For the point cloud the polar coordinates can be converted in Cartesian coordinates with:

$$\begin{bmatrix} x_j \\ y_j \\ z_j \end{bmatrix} = \begin{bmatrix} r_j \sin\theta_j \sin\varphi_j \\ r_j \sin\theta_j \cos\varphi_j \\ r_j \cos\theta_j \end{bmatrix}. \quad (2)$$

Measurement plan

For performing the measurements, there are some time restrictions. Because of the strong reflectivity of the white main reflector, incoming sunlight should be avoided. Thus, the measurements can start only when the sun goes down. However, scanning cannot be performed until the morning because, at some point, dew forms and the water on the surface of the main reflector would affect the measurements.

To capture various positions of the HA-DEC mount telescope, a schedule is set up, including four scanning tours that can be seen in Figure 3. The four tours are scanned on four consecutive nights (from 6 pm to 11 pm, April 2024), beginning with the red one. Each tour consists of 19 to 24 positions that are defined as a combination of hour angle and declination.

To capture a whole tour in one night also an appropriate scanning resolution should be chosen that is

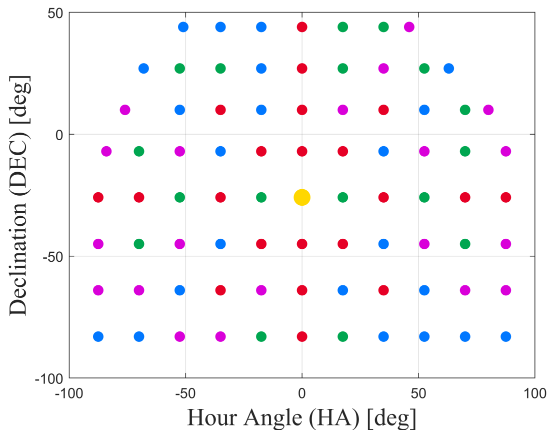

Figure 3. Scanning schedule including four scanning tours: red, green, blue and magenta – yellow represents the zenith position that is captured twice in each tour

fast but dense enough for the analysis. Therefore a resolution of 6.3 *mm* on a range of 10 *m* is chosen, what leads to a scanning duration of around 3 minutes per scan. Some time has also to be taken into account for the movement of the telescope, fixing the brake and set the scan parameters for the horizontal and vertical angle.

2.3 Preprocessing steps

Before estimating the focal lengths and local deviations of the main reflector from the point clouds, the data must be preprocessed to remove unwanted elements. In addition to the main reflector, the scans contain background regions and scatter points that could interfere with the analysis and must, therefore, be eliminated. To achieve this, an automated data-cleaning process in three steps is applied.

In the first step, threshold values are introduced. The maximum distance $D_{\max}$ and minimum distance $D_{\min}$ of the main reflector to the scanner serve as filters to exclude all points outside these limits. The filtering condition is given by:

$$D_{min} \leq r \leq D_{max} \tag{3}$$

The second step involves segmenting the remaining scan into surface patches. These patches are smaller than a single panel and are defined by discretizing the horizontal and vertical angles with step sizes $\Delta\phi$ and $\Delta\theta$. As a result, the entire telescope surface is divided into surface patches of about $30\,cm^2$, which are analyzed individually in the subsequent step.

In the third step, a planar fit is performed for each surface patch. Therefore, RANSAC (RANdom SAmple Consensus) is used. Due to their small size relative to the overall telescope structure, the patches can be approximated as planar surfaces, i.e. planes with parameters A, B, C, D, neglecting the telescope's inherent curvature. Using a predefined threshold, all points P_j deviating beyond a specific limit ε above or below the estimated plane are classified as outliers and removed. All the other points are defined as inlier points P_{inlier} and build the remaining point cloud:

$$P_{inliers} = \{P_j \mid \frac{|Ax_j + By_j + Cz_j + D|}{\sqrt{A^2 + B^2 + C^2}} \leq \varepsilon\}. \tag{4}$$

The final result of preprocessing is a segmentend point cloud that represents only the surface of the radio telescope, free from scatter points (Figure 4).

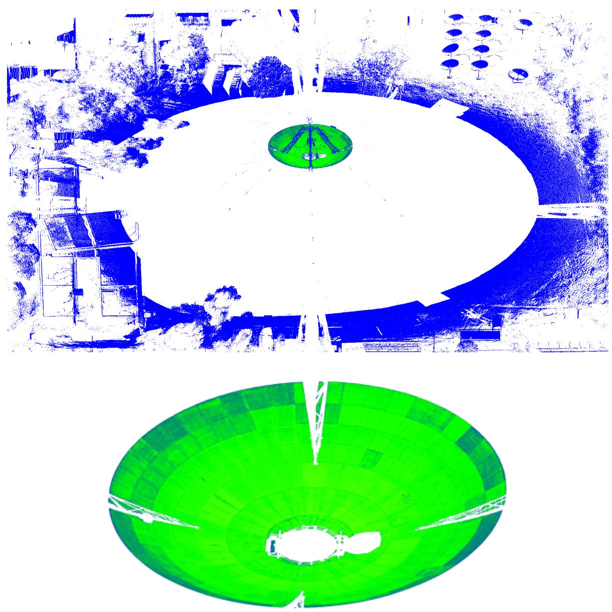

Figure 4. Point cloud with intensity-based coloring (top: whole point cloud; bottom: cleaned point cloud after preprocessing)

3. Workflow for quantifying the reflector deformations

In the following section a workflow is introduced how the preprocessed point cloud can be used to quantify deformations of the main reflector. The laser scan data does not perfectly describe a paraboloid, as represented by the HartRAO telescope model. A least-squares-adjustment is performed to fit the scan data to the model of the telescope. The result of this adjustment is the focal length as the one parameter that accurately describes the overall shape of the paraboloid, along with residuals that also highlight local deformations on the main reflector's surface.

These residuals reflect the differences between the modeled data and a perfect shape. Furthermore, the adjustment can incorporate a calibration process, which allows for the minimization of the systematic errors caused by the misalignments of the laser scanner. As an adjustment is performed for each position, both the focal length variations and the local surface deformations can be described for different positions of the telescope. The workflow for the processing is shown in Figure 5 and will be explained in the following. It needs to be noted that we only focus on the local surface deformations in this publication – focal length variations will be analyzed in future studies.

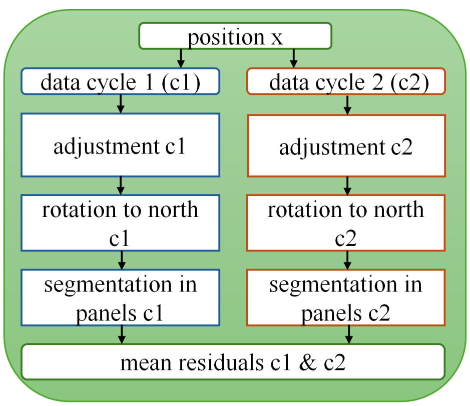

Figure 5. Workflow for processing the point cloud in general - adjustment is done either with the simplified or the extended model

Simplified model

The 26-m HartRAO telescope can be described by

$$\left(\frac{X_j^2+Y_j^2}{4f}\right)-Z_j=0 \tag{5}$$

as a paraboloid of revolution. Here the Cartesian coordinates (X_j,Y_j,Z_j) are represented in the telescope coordinate system. This originates at the vertex of the paraboloid, ensuring that the Z-axis serves as the axis of symmetry (Figure 1). The focal length f is the defining parameter of the paraboloid that uniquely describes its shape (Holst et al., 2017).

A transformation from the scanner coordinate system to the telescope coordinate system must be performed to obtain the coordinates in the telescope reference frame from the raw scanner data. This involves converting the polar coordinates (r_j,φ_j,θ_j) into the corresponding Cartesian coordinates (x_j,y_j,z_j) as Equation 2 shows.

The scanner coordinate system is defined as a right-handed system with its origin at the center of the laser scanner. The scanner and telescope coordinate systems are shown in Figure 1 for the zenith position of the telescope. The blue arrow is the z-axis of the scanner system and points to the nadir, whereas the red arrow shows the Z-axis of the telescope system, which points upwards from the origin of the telescope. In both cases, the x- and y-axes are perpendicular to the z-axis and build a right-handed system. If the telescope moves to another position, this constellation will change. The scanner-z-axis always goes to the nadir. The telescope-Z-axis depends on the telescope's position.

The transformation from the scanner $\mathbf{x}_j$ to the telescope system $\mathbf{X}_j$ can be performed by

$$\mathbf{X}_j=(X_j,Y_j,Z_j)^T=\mathbf{R}_y(\phi_y)\mathbf{R}_x(\phi_x)\cdot\mathbf{x}_j+\Delta\mathbf{X}, \tag{6}$$

which consists of the rotations $\mathbf{R}_x$ and $\mathbf{R}_y$, as well as a translation $\Delta\mathbf{X}$ (Holst et al., 2017).

By integrating the transformed coordinates from Equation 6 into Equation 5, object parameters

$$P_{\text{obj}}=[\Delta X,\Delta Y,\Delta Z,\phi_x,\phi_y,f]^T \tag{7}$$

can be estimated using a least squares adjustment in the form of a Gauss-Helmert model. These object parameters consist of the translation and rotation involved in transforming the scanner reference frame to the telescope reference frame and the focal length of the paraboloid (Holst et al., 2017). Until this step, we speak about the simplified model.

Extended model

In a further step, the functional model can be extended to model systematic errors that can be related to the laser scanner misalignments. In this case, the parameters are augmented with calibration parameters P_{calib} in addition to the object parameters P_{obj} of Equation 7:

$$P_{\text{calib}}=[x_4,x_6,x_7]^T. \tag{8}$$

Here, x_4 represents the vertical index offset, x_6 denotes the mirror tilt, and x_7 corresponds to the horizontal axis error. As noted in Holst et al. (2017), the calibration parameters significantly impact the results. The calibration parameters are added to the raw data $(r_{orig}, \varphi_{orig}, \theta_{orig})$:

$$\begin{bmatrix} r_j \\ \varphi_j \\ \theta_j \end{bmatrix} = \begin{bmatrix} r_{\mathrm{orig}_j} \\ \varphi_{\mathrm{orig}_j} + \frac{x_7}{\tan(\theta_j)} + \frac{2x_6}{\sin(\theta_j)} \\ \theta_{\mathrm{orig}_j} + x_4 \end{bmatrix}. \tag{9}$$

Transformation in consistent coordinate system

In the next step, the adjusted coordinates are transformed to ensure they are represented in the correct telescope reference frame where the X-axis represents the north direction. Since the coordinate system, after adjustment, already has its origin at the vertex of the main reflector and the Z-axis is correctly oriented, only a rotation around the Z-axis is necessary to also correctly orient the X- and Y-axes. This procedure is done for each cycle in each position separately. For each position, cycles 1 and 2 are divided into 255 panels, with the edges removed by using a defined mask to eliminate potential overlaps between adjacent panels.

To combine cycle 1 and cycle 2 and to compensate for any remaining systematic effects caused by laser scanner misalignments, the residuals from the two cycles are averaged panel by panel in a final step. Therefore, points within a panel are grouped into circles with their nearest neighbors where the circle has a radius of about 1 *cm*. Points within one circle are averaged. Since the edges of the panels were cut in the previous step and the calculation is done panel-by-panel, it can be ensured that points of two different panels are never averaged.

4. Preliminary analysis and discussion of residuals

This section shows and discusses the results of the simplified model compared to the extended model, which includes calibration parameters. We group this analysis into scans in which misalignments have been reduced successfully and into scans that contain a large amount of systematic errors even after the process of calibration using the extended model. Those overlying systematics with previously unknown appearance will be explained later. In this study, since we only analyze first results, we restrict the further discussion to the red tour only (compare Figure 3).

4.1 Scans with successful reduction of misalignments

As the residuals are a main part of the deformation analysis, because they show the local deformations of a radio telescope's main reflector, particular attention is put on the reduction of systematic errors that affect the residuals directly. To show the effects of modeling the systematic errors as a calibration included in the adjustment (i.e., extended model), the scan data is processed along the workflow in Figure 5 once with the simplified model and once with the extended model.

When applying the simplified model, the residuals clearly reveal the influence of systematic errors as a

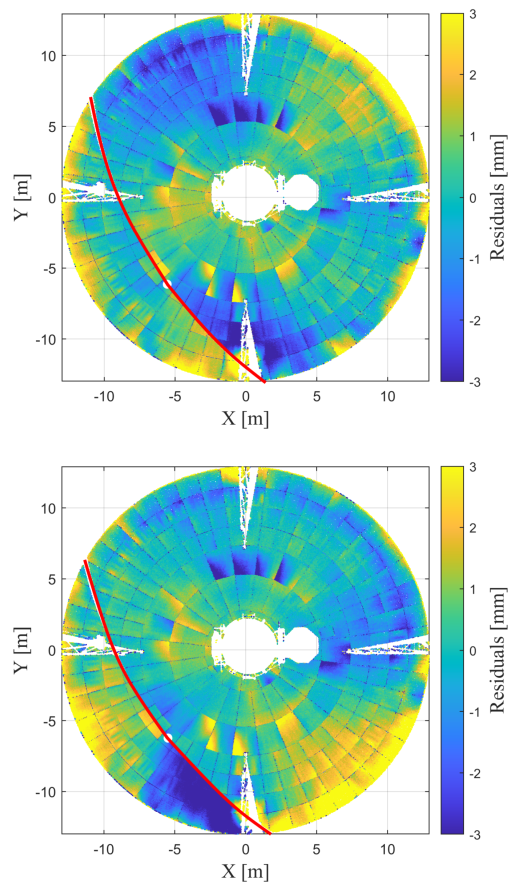

Figure 6. Residuals of the deformation analysis without calibration parameters r23 (HA: $-35°$, DEC: $-64°$ - red line separates face 1 and 2 (top: cycle 1; bottom: cycle 2)

visible line shown as a red line between face 1 and face 2 (Figure 6). This can be observed for both cycles 1 and 2. Since cycle 1 covers a horizontal angle range from 0° to 180° and cycle 2 from 180° to 360°, the regions corresponding to face 1 and face 2 and further the systematic effects are interchanged between the two cycles.

Applying the extended model including the calibration parameters leads to a significant improvement, as the systematic effects are minimized (Figure 7). However, a closer inspection of cycles 1 and 2 in Figure 7 reveals smaller but persistent discontinuities in the residuals along the face changes that hint at remaining systematic instrumental effects. To deal with this issue, a panel-wise averaging of cycles 1 and 2 is done to build the mean of face 1 and face 2.

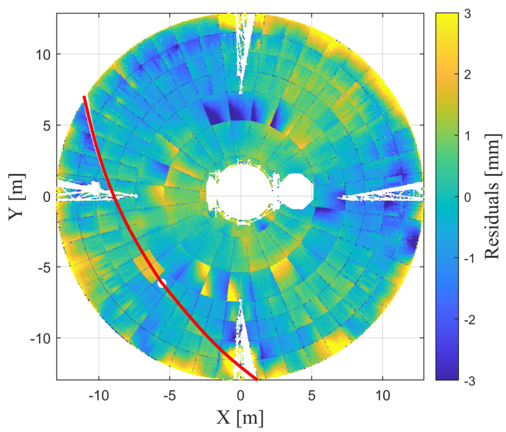

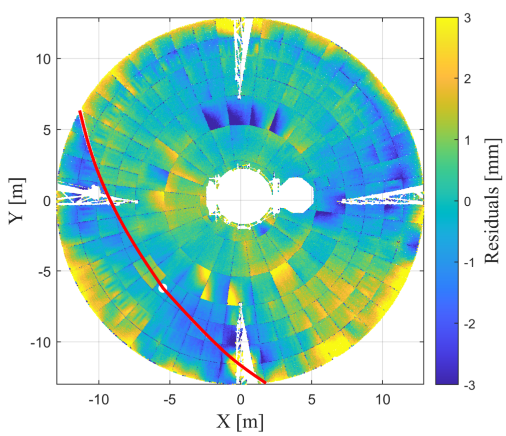

Figure 7. Residuals of the deformation analysis with calibration parameters r23 (HA: −35°, DEC: −64° - red line separates face 1 and 2 (top: cycle 1; bottom: cycle 2)

The results of this averaging method including calibration are shown in Figure 8. Significantly fewer systematic effects are visible. The residuals represent local deformations or deviations of the telescope from a perfect paraboloid, potentially indicating tilted, dented or even wholly shifted panels. The region around the right quadruped leg shows panels below the paraboloid's perfect shape. Also, three panels below the top quadruped leg show the same behavior and are tilted.

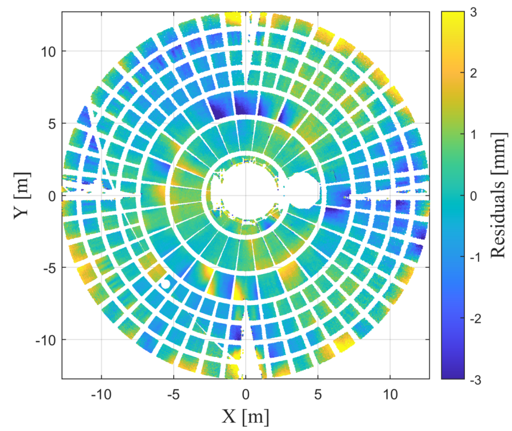

Figure 8. Mean residuals of the deformation analysis for r23 (HA: −35°, DEC: −64°) with calibration

4.2 Scans with overlaying systematics

For most of the scans, the residuals and therefore the local deformations look quite similar after analysis including calibration and building the mean of the two cycles. However, some scans show a completely different behavior in the residuals that does not fit the local deformations and is not related to two-face-sensitive systematic errors. This abnormal behavior can be found in four of the 46 scans, always in the first of the two cycles. Figure 9 shows one of the affected scans. These effects appear either in the last or in the first quarter of the scan.

A clear line is visible in the residuals as a clear contrast between blue and yellow. On the one hand, the systematic influences of the laser scanner, which are two-face sensitive, are distinctly visible in Figure 9 shown with the solid red line. This line is along the horizontal angle of 0°. On the other hand, abnormal effects can be observed within the black dotted line along one random horizontal angle.

For the four detected abnormal scans, there is not yet a relation or systematic found for the position of the effects. With a closer look at the raw data, these effects can also be detected as a shift perpendicular to the telescope's surface along one horizontal angle value. However, since these abnormalities occur at different locations in only four scans, it can be ensured that they do not represent actual deformations on the main reflector's surface.

The exact cause of this influence remains unclear. Still, these anomalies consistently occur in the first cycle of the examined scans. This observation suggests that the brake may not have been fully engaged or that the telescope had not yet completely settled after moving into position. This could have caused a momentary impulsive shift, which manifests along the line of a specific horizontal angle. Since these scans are affected by erroneous influences, they should not be used for further evaluation and therefore be excluded from the subsequent analysis or even the affected parts have to be cut out of the point clouds.

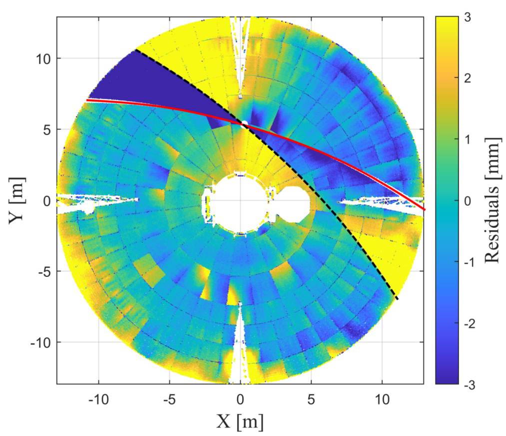

Figure 9. Residuals with abnormal effects of point cloud in position r5 (HA: 35°, DEC: $-25.89°$) cycle 1 - red line separates the systematic errors, black line the abnormal effects

5. Conclusion

For the preliminary results, it can be summarized that a sophisticated measurement concept was designed enabling to analyze the deformation behavior of the HartRAO 26-m radio telescope in its full working range. Furthermore, we set up a workflow that segments the scan data in an almost automatic way. It is shown that an included calibration in the adjustment improves the quality of the adjusted data a lot as the systematic errors are almost eliminated. In most of the cases, these effects can be modeled in a reliable way. Anyway, there are some scans in which unknown systematic effects appear that cannot yet be explained or modeled.

In further steps, we will focus on modeling also the unknown systematic effects and also analyze the resulting focal length variations. By combining the results of all 88 scans measured in four distinct tours, we will gain a parametric model for all gravitational surface deformations of the main reflector.

Funding

This research was partly funded by German Research Foundation (DFG) under grant number 490989047, DFG FOR 5455 "TLS-Defo".

References

Clark, T. A. and Thomson, P. (1988). Deformations in vlbi antennas: Goddard space flight center, maryland. *NASA Technical Memorandum 100696*.

Holst, C. and Kuhlmann, H. (2014). Aiming at self-calibration of terrestrial laser scanners using only one single object and one single scan. *Journal of Applied Geodesy*, 8(4).

Holst, C., Medic, t., Nothnagel, A., and Kuhlmann, H. (2019a). Analyzing shape deformation and rigid body movement of structures using commonly misaligned terrestrial laser scanners: the radio telescope case. *4th Joint International Symposium on Deformation Monitoring (JISDM),15-17 May 2019, Athen, Greece*.

Holst, C., Nothnagel, A., Haas, R., and Kuhlmann, H. (2019b). Investigating the gravitational stability of a radio telescope's reference point using a terrestrial laser scanner: Case study at the onsala space observatory 20-m radio telescope. *ISPRS Journal of Photogrammetry and Remote Sensing*, 149:67–76.

Holst, C., Schunck, D., Nothnagel, A., Haas, R., Wennerbäck, L., Olofsson, H., Hammargren, R., and Kuhlmann, H. (2017). Terrestrial laser scanner two-face measurements for analyzing the elevation-dependent deformation of the onsala space observatory 20-m radio telescope's main reflector in a bundle adjustment. *Sensors (Basel, Switzerland)*, 17(8).

Lösler, M., Eschelbach, C., Greiwe, A., Zhou, B., and McCallum, L. (2025). Innovative approach for modelling gravity-induced signal path variations of vlbi radio telescopes. *Earth, Planets and Space*, 77(1).

Lösler, M., Haas, R., Eschelbach, C., and Greiwe, A. (2019). Gravitational deformation of ring-focus antennas for vgos: first investigations at the onsala twin telescopes project. *Journal of Geodesy*, 93(10):2069–2087.

National Research Fundation (2025). Hartrao 26m radio telescope details.

Nothnagel, A. (2009). Conventions on thermal expansion modelling of radio telescopes for geodetic and astrometric vlbi. *Journal of Geodesy*, 83(8):787–792.

Nothnagel, A., Zhihan, Q., Nicolson, G. D., and Tomasi, P. (1994). Earth orientation determinations by short duration vlbi observations. *Bulletin Géodésique*, 68(1):1–6.

Sarti, P., Vittuari, L., and Abbondanza, C. (2009). Laser scanner and terrestrial surveying applied to gravitational deformation monitoring of large vlbi telescopes' primary reflector. *Journal of Surveying Engineering*, 135(4):136–148.